JOURNAL OF MATERIALS SCIENCE 16 (1981) 739–751

Correlation of hardness and microstructure in unoriented lamellar polyethylene

F. J. BALTÁ CALLEJA, J. MARTINEZ SALAZAR
Instituto de Estructura de la Materia, CSIC, Madrid 6, Spain

H. ČAČKOVIĆ, J. LOBODA-ČAČKOVIĆ
Fritz Haber Institut der MPG, Teilinstitut für Strukturforschung Berlin, Germany

The local deformation of the lamellar microstructure of isothermally melted crystallized unoriented polyethylene has been investigated using microindentation hardness (MH). The polymer can be visualized as a composite material consisting of hard and weak elements. The former, the lamellae, are considered to consist of mosaic blocks with liquid-like lattice distortions (paracrystallites). The latter are the interlamellar "amorphous" regions and the mosaic block lateral grain boundaries. The deformation mechanisms beneath the indenter are discussed in the light of current models of plastic deformation. MH is shown to depend on the packing density of the macromolecules in both phases and, as a result, it can be clearly correlated with the macroscopic density of the material. The unit cell expansion and lattice distortions increase in parallel as a consequence of increasing incorporation of chain defects within the lattice. This provokes a conspicuous decrease in the microhardness of the crystals. The increase in lattice distortions is consistent with the concurrent decrease of lamellar thickness and, hence, of the coherently diffracting lattice volume. These results unambiguously emphasize the physical significance of the mosaic block character of the lamellae in determining the micromechanical properties of the material. Finally it is shown that the strain boundary which defines the zone of crystal destruction under the indenter also depends on the average volume of the paracrystallites and on the volume fraction of crystalline material.

1. Introduction

In contrast to the systematic hardness investigations of metals and alloys of the last 40 years [1, 2] which offer a well established picture of the fundamental mechanisms involved in hardness, this study of indentation hardness of polymeric materials is more recent and has been mainly focused on topics of applied significance [3–7]. The latest studies on the microhardness (MH) of semicrystalline polymers have, nevertheless, been useful in pointing out different microstructural mechanisms occurring at various morphological levels [8–13]. This is possible because microindentations can be made small enough (a few μm in depth for a few g load) to respond to specific changes in microstructure. MH testing can, for instance, unambiguously detect the local strain hardening observed in a polymer after plastic deformation which parallels the discontinuous transition from the initial microspherulitic to the final fibre structure [9]. MH is also an increasing function of annealing temperature – and consequently of chain extension – in oriented chain extended polyethylene (PE) [10]. The micromechanical behaviour of ultradrawn PE fibres has been, furthermore, characterized by taking into account the morphological differences between the outer sheath and the inner core of highly oriented PE strands [12, 13]. In addition, the MH test has been most efficiently used as a tool for the determination of the varying microstructure details of injection moulded thermoplastics [8, 11].

Since the indentation process at the surface of the solid involves both elastic effects and plastic

0022–2461/81/030739–13$03.30/0

TABLE I Molecular weight, defect concentration, crystallinity and microhardness of the samples investigated

Sample	$\bar{M}_n$ ($\times 10^3$)	$\bar{M}_w$ ($\times 10^3$)	ϵ (%)	$\Delta T \sim 10°$ C		$\Delta T \sim 68°$ C	
				α (%)	MH (MN m^{-2})	α (%)	MH (MN m^{-2})
Marlex 6015	–	150.00	0.19	79.7	84.7	62.0	70.5
Hostalen GF	–	120.00	0.70	62.1	72.8	55.5	53.6
Lupolen 1051	–	51.00	1.76	50.5	37.2	47.1	26.2
Epolene N-12	2.10	11.55	2.63	43.5	45.2	56.4	39.5
Lupolen 1810 H	–	54.00	3.04	42.1	20.0	38.7	18.1
Epolene C-13	11.30	284.50	3.61	36.8	16.6	40.6	11.9
Epolene C-10	6.50	20.95	4.77	31.0	12.5	34.2	9.5
Epolene C-101	4.35	18.30	5.34	36.8	15.8	26.6	12.5
Epolene C-12	4.00	11.00	6.90	23.4	6.9	21.3	4.4

yielding under the stress field of the indenter the MH value is admittedly correlated to the specific modes of deformation in polymers. Much attention has been given lately to understanding the relevant mechanisms of plastic deformation of semi-crystalline polymers and a detailed molecular interpretation has been made [14]. The deformation mechanisms in polymers are predominantly determined by the arrangement and structure of microcrystals and their connection by tie molecules. In contrast to low molecular weight substances, built up by an agglomeration of randomly oriented crystallites, polycrystalline polymeric solids show up a conspicuous lamellar morphology [15]. Such a flat shape favours parallel packing into crystal stacks which usually develop into spherulites, in which the lamellae are radially oriented with the molecular chains perpendicular to the radius. This structure results from slow cooling or isothermal crystallization of the melt. The quenched or rapidly cooled, melt results, on the other hand, in randomly oriented stacks of parallel lamellae with no macroscopic orientation which can be considered as incipient spherulitic embryos. The stacking of parallel lamellae produces a local ordering and orientation in a range of a few lamellae thickness (~ 0.1 to $1\,\mu$m) which shows up in the small angle X-ray scattering (SAXS) region. The wide angle X-ray diffraction (WAXD) maxima suggest, furthermore, that the crystalline lamellae consist, in fact, of mosaics of blocks, with liquid-like lattice distortions, which can be defined as "microparacrystals" [16, 17].* These distortions are admittedly produced by the presence of kinks (step chain defects), branches and other conformational irregularities [20] within the crystal lattice. In the case of a low density PE it has been pointed out [21–23] that a given fraction of branches and other molecular defects are rejected from the microparacrystallites, depending on the overall number of such defects along the chain, their size and the plastic deformation of the solid.

The main concern of this paper is the study of the influence of various microstructural parameters, such as the dimensions of the crystalline unit cell, the thickness of the lamellae and the lateral dimensions of the coherently diffracting domains on the microhardness value. In order to cover a wide range of structural parameters PE samples with varying concentrations of chain defects were selected and subsequently crystallized in either of two different supercooling steps. Since the indentation test, local yield involving a permanent change of shape, presumably involves a local destruction of the crystallites at the surface, the present study, based on thermodynamic considerations, attempts a calculation of the volume of "crystalline" material which is thought to be destroyed under the indentor. The influence of geometrical and morphological factors on the volume of the zone of crystal destruction is also examined.

2. Materials and methods

2.1. Sample preparation

A series of commercial samples of PE with a wide range of chain defect concentrations (from 0.17 to 6.9%) were used in this study (Table I). According to i.r. analysis the branches are butyl or longer methylene sequences [24]. The total number of defects, ϵ, is given as the sum of branches plus the

*It is noteworthy, however, that the interpretation of diffraction results has been the subject of certain disagreement [18, 19].

number of unsaturated bonds [25]. These materials were pressed and cast from the melt in the form of plates of 20 mm x 18 mm x 1.5 mm in size, and supercooled at either $\Delta T = 10$ or 68° C. The crystallization procedure was as follows [17]. The samples were melted in sample holders at 160 to 170° C, within a few minutes and subsequently transferred to a silicon oil bath at a chosen temperature. Two crystallization modes were adopted: (a) the temperature of the oil bath was kept at a temperature close to the melting point, T_m. It was then cooled in 2° C steps, each stage being equilibrated for 30 min, until the beginning of crystallization was visually observed. (Independent dilatrometric measurements indicate that the onset of crystallization visually observed corresponds to ~ 10% transformation of the material.) The sample was then allowed to crystallize at this latter temperature for 3 days. Values of $\Delta T =$ 10° C are encompassed in these experiments. The temperature was subsequently reduced in a 10° C step and the sample held for 24 h at this temperature. Finally it was cooled to room temperature at a rate of about 1° C min^{-1}; (b) the second mode ($\Delta T = 68°$ C) consisted of directly dipping the melted polymer into the oil bath at $T_c = T_m -$ 68° C. Here a substantial part of the crystallization was evidently complete before the sampled reached the temperature of the bath. (T_c is the crystallization temperature.)

For the microindentation experiments surface polishing of the samples with a 1 μm diamond paste was used to improve focusing.

2.2. X-ray diffraction techniques

Morphological properties were investigated by SAXS and WAXD measurements. The SAXS patterns were obtained at room temperature with a Rigaku Denki camera using point collimation and a rotating anode X-ray generator. Exposure times of 6 to 34 h were used for all samples with a specimen-film distance of 400 mm. Densitometer traces of the X-ray films were recorded using a Joyce and Loebel two beam microdensitometer. The long periods were calculated according to Bragg's equation from the first maximum of the scattering intensity after subtraction of the background. The unit cell dimensions determination and the wide angle line broadening measurements were made by step scanning using the first fifteen crystalline peaks of PE (1 1 0, 2 0 0, 2 1 0, 0 2 0, 1 2 0, 0 1 1, 3 1 0, 1 1 1, 2 0 1, 2 2 0, 2 1 1, 4 0 0, 1 2 1, 3 1 1 and 2 2 1) on a powder diffractometer with Ni filtered CuKα radiation. Si was used as the instrumental standard. Other details of the experimental procedure were described earlier [17, 26]. The volume fraction of crystallized material, α, was determined by the X-ray method described by Vonk [27].

2.3. Determination of crystallite size amd lattice imperfections

One may expect that the critical stress (yield point) needed to plastically deform the lamellar structure of the polymer will be dependent, to some extent, on intermolecular forces, degree of lattice perfection and crystal thickness. These are the morphological parameters that we set out to correlate to MH. The required information about the chain packing within the crystals and the dimensions of the basic subunit, the lamellae, was obtained from WAXD and SAXS respectively. These techniques measure only average properties and cannot reveal non-representative lamellar features in detail [15]. From the long period, L, of the crystal stack assuming a sandwich concept, crystal core and amorphous surface layer, the crystal thickness, l, was derived from: $l = L\alpha\rho/\rho_c$, where ρ is the density of the samples and ρ_c is the crystalline density. Values of paracrystalline lattice fluctuations (g) and the size of the coherently diffracting domains, D_{hk0}, normal to the chain axis were obtained, according to the paracrystal theory [28], from the integral width of the reflections

$$\delta\beta_{hk0} = \frac{1}{D_{hk0}} + \frac{(\pi g)^2}{\bar{d}_{hk0}} m^2 \qquad (1)$$

where m is the order of the reflection, $\bar{d}_{hk0}$ the average lattice spacing and $g = \Delta d/\bar{d}_{hk0}$, where Δd is the mean statistical fluctuation between the lattice planes. This expression assumes that the lattice distortions and the shape factor are Lorentzian. This is approximately valid for other profiles. The density of chain defects, ϵ_c, which are incorporated within the lattice per 100 carbon atoms was calculated assuming a chain defect accommodation by generation of a $2g1$ kink according to the expression [21]:

$$\epsilon_c = (V_\epsilon - V_0)/4\Delta V \qquad (2)$$

where V_ϵ is the unit cell average volume of a sample with ϵ defects, V_0 is the unit cell volume for $\epsilon = 0$ and $\Delta V \sim 60$ Å^3 is the excess volume of

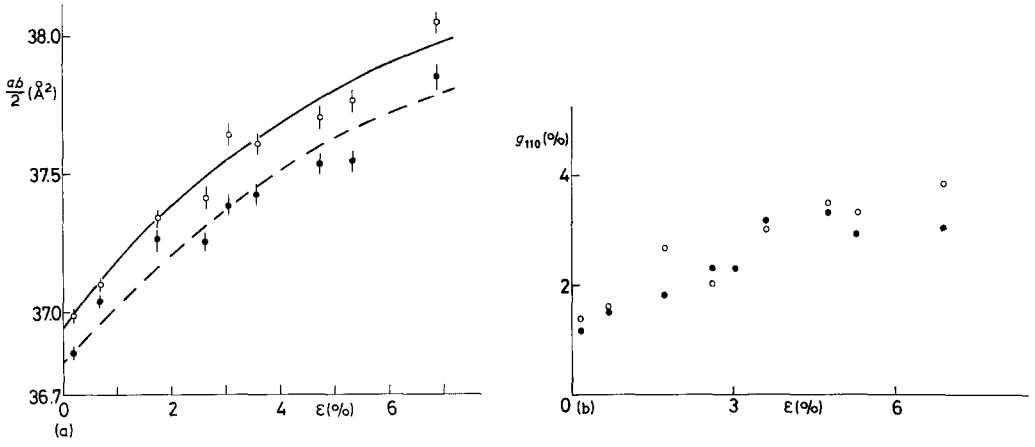

Figure 1 Parallel increase of (a) the PE molecular cross-section and (b) the paracrystalline lattice distortions orthogonal to the (1 1 0) planes for low density PE samples crystallized at 2 supercoolings of (○) $\Delta T \simeq 10°$ C and (●) $\Delta T \simeq 68°$ C as a function of the concentration of defects ϵ.

each kink associated with a CH_2 group in the crystal. A recent statistical approach [29] based on crystallinity and crystal thickness data confirms the defect inclusion data obtained using Equation 2. The density of defects localized on the amorphous layer and at the mosaic block grain boundaries was calculated from

$$\epsilon_a = (\epsilon - \alpha\epsilon)/(1 - \alpha). \quad (3)$$

2.4. Density measurement

The density, ρ, of the samples was determined at room temperature by the column gradient density method in a mixture of p-xylene (81%) and carbon tetrachloride (19%). The density measurements are believed to be accurate to ± 0.0005 g cm^{-3}. The crystalline density, ρ_c, was calculated from the crystalline unit cell dimensions. The standard errors in the dimensions correspond to a standard deviation of 0.001 g cm^{-3}. The amorphous density, ρ_a, was derived by assuming a two phase concept from [30]

$$\rho_a = (1 - \alpha)/(\rho^{-1} - \alpha\rho_c^{-1}). \quad (4)$$

2.5. Microhardness testing

The MH measurements were carried out at room temperature with a Leitz tester using a Vickers square pyramidal diamond. The dimension of the diagonals, d, of the observed diamond shaped indentation was measured immediately after load removal with a micrometer eyepiece of the microscope. The accuracy of the measurements were $\pm 0.5\,\mu$m. The immediate elastic recovery was undetectable within experimental error. For further details see [12]. The hardness value was therefore calculated from the projected area of indentation according to

$$\mathrm{MH} = k\frac{p}{d^2}(\mathrm{MN\,m^{-2}}) \quad (5)$$

where d is the length of the indentation diagonal in μm, p is the load applied in g and k a geometrical factor equal to 18.191×10^3. Measurements were carried out with a load of 15 g. The final permanent deformation was a function of the length of contact time under load. The loading cycle was controlled at various times between 0.1 and 20 min. Each indentation was repeated 10 times for $t < 5$ min and 3 times for $t > 10$ min. Care was taken with the method of specimen mounting and illumination. The recommendations of Bowman and Bevis [11] were followed. Possible edge effects, indentation interactions as well as eventual influence of work hardening was likewise avoided.

3. Results

The influence of chain packing in PE crystals is significantly affected by the inclusion of chain defects and by the crystallization conditions. Fig. 1a, illustrates the conspicuous expansion of the PE molecular cross-section, $axb/2$, as a function of chain defect content for the two different supercoolings. The molecular cross-section shows, indeed, a first rapid increase in the region $0 < \epsilon < 1.5\%$ with a slower increase rate for $\epsilon > 3\%$. This behaviour is similar to that reported by Swan [31] for bulk PE co-polymers, by Holdsworth and Keller [32] for solution crystallized material and

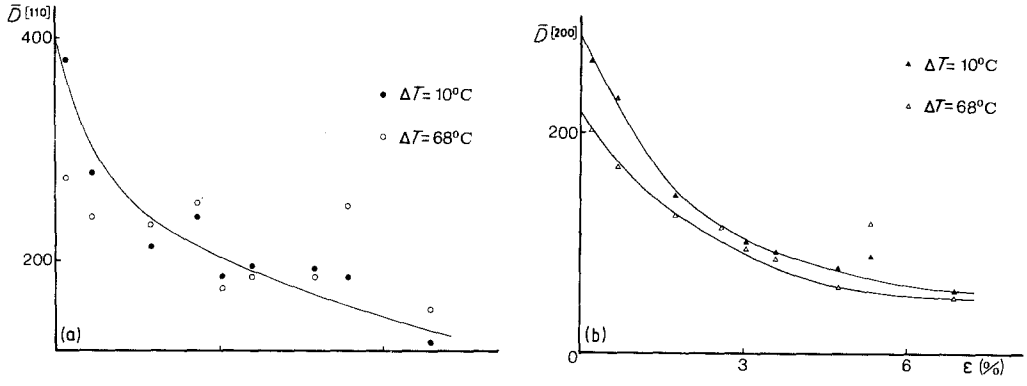

Figure 2 Crystal size decrease orthogonal to (a) the (1 1 0) and (b) the (2 0 0) net-planes as a function of decreasing ϵ.

to our own observations performed with samples crystallized during cooling [21]. The supercooling dependence of the unit cell expansion was previously established by Davis *et al.* [33] for linear PE. Parallel to the unit cell expansion observed, the value of the paracrystalline distortions, g_{110}, gradually increases from 1 to 1.5% for $\epsilon \sim 0.2$ up to values in the vicinity of $\sim 4\%$ for $\epsilon \sim 7\%$ (Fig. 1b). On the whole the g_{110} values seem to be larger for the samples crystallized in higher supercoolings. The mosaic block dimensions, D_{hkl} decrease with increasing ϵ for the two supercoolings under investigation (Fig. 2). In addition, it is worth noting that the value of D_{200} decreases more rapidly than D_{110} with ϵ. This is a result of the anisotropy increase of the microparacrystallites with increasing concentration of chain defects. The increase of the paracrystalline lattice fluctuation and the decrease of the coherently diffracting domains closely follows the law

$$(D/\bar{d})^{1/2} \cdot g \mid = \alpha^* \qquad (6)$$

where α^* is a dimensionless constant. This supports the concept of a real paracrystal [34]. This is a result of the limiting size which is reached by the mosaic blocks, as a consequence of the increasing built-in defects, causing the statistical fluctuations between adjacent lattice planes to reach the order of magnitude of a net-plane separation $\bar{d}$. For the samples investigated α^* varies between 0.1 and 0.2. Paracrystalline distortions in polymers are admittedly produced by the three-dimensional incorporation of step chain defects, such as kinked isomers, within the lattice disturbing the crystalline regularity [16, 35]. The density of chain defects, ϵ_c, which are incorporated in the lattice per 100 carbon atoms, according to Equation 2 is shown in Fig. 3. Slightly larger values of ϵ_c for the samples crystallized at a higher supercooling appear. The increasing incorporation of defects within the lattice with ϵ provokes a decrease of the crystalline density exhibiting higher ρ_c values at a lower supercooling (Fig. 4). In spite of the detectable inclusion of defects within the lattice the data shown in Fig. 3 unambiguously emphasize the conspicuous major exclusion of chain defects from the crystals for all values of ϵ. The decrease in density of the amorphous phase, ρ_a, with ϵ is, hence, much more notable than that of ρ_c as illustrated in Fig. 4. Thus, ρ_a decreases from 0.965 down to 0.88 g cm^{-3} for the samples with $\Delta T = 10^\circ$ C and from 0.90 to 0.87 g cm^{-3} for the samples with $\Delta T \sim 68^\circ$ C. These results are evidently in agreement with the suggested preferential exclusion of defects from the crystalline lattice. This exclusion of chain defects, therefore, increases with the increasing overall number of defects along the molecular chains. These changes are accompanied, as illustrated in Fig. 5, with a parallel decrease of L and l with increasing ϵ. The decrease of l with ϵ is, however, larger than the average separation ($l = \epsilon^{-1} \times 1.27$ Å) between adjacent branches along the polymer chain. For both supercoolings the difference $a = (L - l)$, which is related to the thickness of the disordered layer surface of the crystals increases with the increasing concentration of defects.

A salient feature concerning the surface mechanical properties is the creep effect shown by these PE samples, i.e. the time dependent part of the plastic deformation of the polymer under the stress of the indenter. A very detailed phenomenological description of macroscopic creep was given not long ago by Ehrestein [36]. The creep curves are characterized by a decreasing strain rate, which can be described by a time law of the form

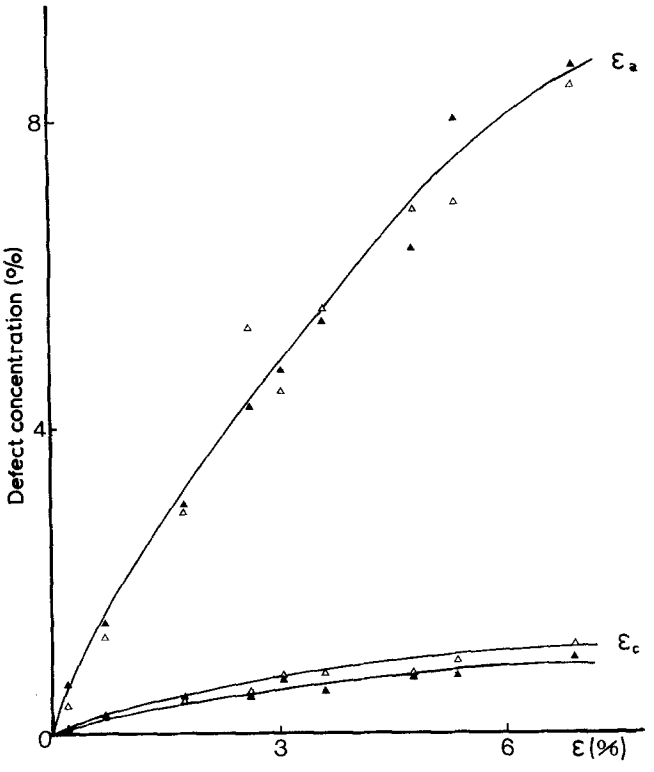

Figure 3 Defect concentration within the "crystals", ϵ_c, from Equation 2 and in the "amorphous" regions, ϵ_a, for the ϵ range investigated, ▲ at $\Delta T \sim 10^\circ$ C and △ at $\Delta T \sim 68^\circ$ C.

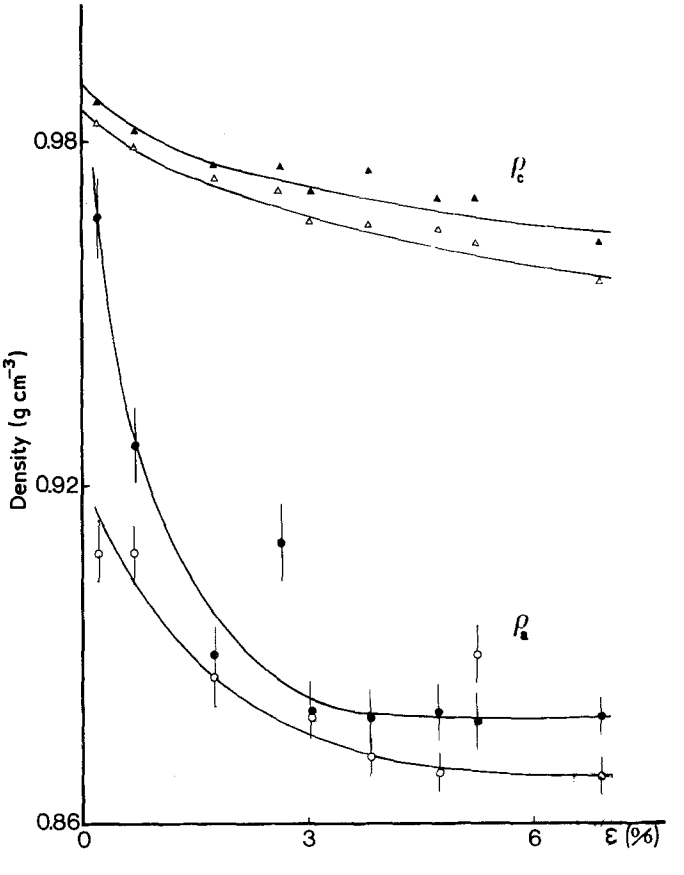

Figure 4 Crystalline, ρ_c, and amorphous density, ρ_a, as a function of increasing defect concentration ϵ, ▲ and ● at $\Delta T = 10^\circ$ C and △ and ○ at $\Delta T = 68^\circ$ C.

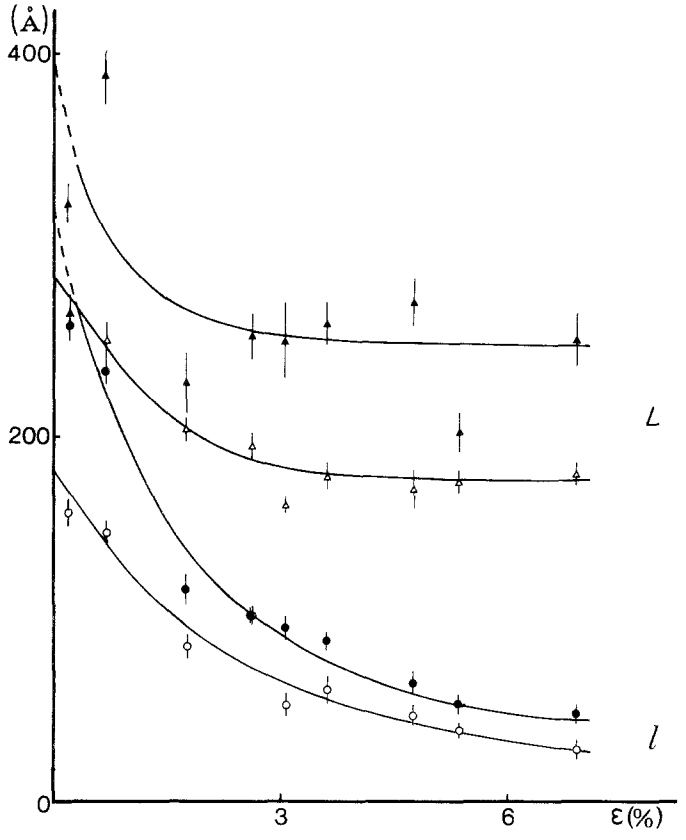

Figure 5 Long period, L, and crystal thickness, l, decrease as a function of total defect concentration ϵ, ▲ and ● at $\Delta T \sim 10°$ C and △ and ○ at $\Delta T \sim 68°$ C.

$MH = At^{-K}$. The constant A is a coefficient which depends on temperature and loading stress and K is a constant which provides a quantitative measure of the rate of creep of the material. A MH value of 0.1 mm has been adopted in this study because it approaches Tabor's relation ($H = 3Y$, where H is hardness and Y is yield stress) [1]. The constant K, at least for the linear polymer, has been shown to depend on ΔT($K = 6.8 \times 10^{-3}$ for $\Delta T = 10°$ C and $K = 13 \times 10^{-3}$ for $\Delta T = 68°$ C). This result indicates that creep presumably depends among other factors upon crystallinity and crystal perfection. The values of microhardness $MH_{0.1}$ obtained are collected in Table I together with the simultaneous decrease of α with increasing ϵ. As shall be discussed below, MH is strongly dependent not only on the average chain packing within the unit cell and on the lattice distortions present, but also on the lamellar thickness and lateral dimensions of the paracrystals.

4. Discussion

4.1. Influence of morphology on microhardness

Polymeric materials are most frequently used in technology in the isotropic form. One aim of the present work is to explain and possibly to predict microhardness of isotropic lamellar polymers like polyethylene. The unoriented semicrystalline polymer may be regarded for many purposes as a composite material consisting of separate and mechanically distinct "strong" (crystalline) and "weak" (disordered) elements. Given the geometrical arrangement of these two phases, and this clearly involves more than a mere knowledge of their volume fractions, and given the hardness of these phases, the problem is to predict the hardness value of the material. The application of composite theories to relationships between mechanical properties and microstructure in semicrystalline polymers is based on the assignment of ideally constant mechanical properties to the microstructural elements of the polymeric solid [37]. In the actual sample the crystal lattice is, however, not ideal but contains all types of crystal defects and nor is the non-crystalline component ideally amorphous. Hence, the density of the former is less than the ideal crystallographic density ρ_c and that of the latter is larger than ρ_a, the density of the ideal supercooled melt. The observed variation of the values of ρ_a and ρ as a function of ϵ (Fig. 4) suggests, in fact, a distinct

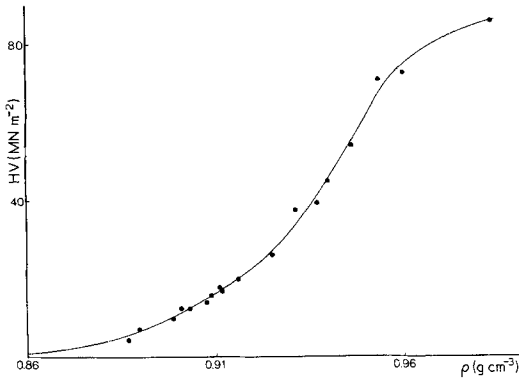

Figure 6 Dependence of microhardness on macroscopic density using a load of 15 g and a loading time (t = 0.1 min).

varying packing density of the macromolecules in the two phases which decreases with increasing ϵ and ΔT. Microhardness must be, consequently, a function of both ρ_a and ρ_c, and, as a result, also of ρ. Density is a crystallinity parameter which has been previously correlated with success to the mechanical behaviour of polymers [38–40] (yield stress, elastic modulus). Fig. 6 illustrates the conspicuous unequivocal increase of MH as a function of ρ. On account of the density data on Fig. 4 three distinct regions can be distinguished in Fig. 6.

(1) MH values which are between 5 and 30 MN m^{-2} mainly correspond to densities close to those of the "amorphous" domains. Plastic deformation in this case will probably be preceded by preferential compression of disordered molecular regions. Resistance to deformation occurs largely due to resistance to bond rotation [41]. The chains randomly kinked can be elongated if rotation takes place about certain bonds in the chain backbone. Work has to be done against the steric hindrance to rotation.

(2) In the region of MH $>$ 80 MN m^{-2} (densities close to the crystal unit cell density) the deformation modes of the crystals must predominate. The strong elements of the solid are lamellae consisting of paracrystalline mosaic blocks. The mechanical properties in this case are primarily determined by the large anisotropy of the molecular forces i.e. strong –C–C– covalent bonding in the chain direction and weak van der Waals forces between close packed chains, favouring longitudinal chain displacement. Chain slip and tilt leading to lamellar shear allow large deformation of the crystalline blocks. The mosaic structure of the blocks with an imperfect lattice fit at the block boundary introduces a specific weakness element which permits chain slip to proceed faster at the block boundaries than inside the blocks. The weakest element of the solid is certainly the surface layer between adjacent lamellae, containing chain folds, free chain ends and tie molecules.

(3) MH values between 30 and 80 MH m^{-2} can be considered as typical for the semicrystalline solid (ρ shows values between ρ_a and ρ_c). Here, most probably, crystalline and amorphous deformation modes contribute equally to MH.

When the polymeric material is compressed the local deformation beneath the indenter will consist of a complex combination of effects. The specific mechanism prevailing will depend on the strain field depth round the indent and on the morphology of the polymer.

According to the various mechanisms of plastic deformation proposed for semicrystalline polymers [14, 42] the following effects may be expected: (a) on the one hand, eventual phase transformations or twinning within the lamellae [43] and probably elastic bending of crystals [44] involving small strains ($<$ 10%) (i.e. at depths of the order of 1d); (b) inter-lamellar sliding and separation involving shearing and compressional deformation of the amorphous layers and destruction of some blocks at slightly larger strains (10 to 20%); (c) lamellar fracture at the block boundaries while chains bridging the fractured blocks become partially unfolded and finally total co-operative block destruction at very large strains [42, 45] ($>$ 20%) i.e. at depth $<$ 0.5d (see Fig. 7). When the magnitude of the stress reaches the yield point a macroscopic local plastic deformation is produced. The material beneath the indenter becomes permanently displaced and a micro-impression arises; (d) when the applied stress field is removed, the molecules in the amorphous layers and the tie molecules acting as crosslinks between adjacent more or less fractured crystals tend slowly to relax back. Fig. 8 schematically illustrates a suggested model of plastic deformation of the compressed lamellae beneath the indenter.

The MH of such a composite material can be approximated to

$$\mathrm{MH} = \alpha H_c + (1 - \alpha) H_a \qquad (7)$$

where H_c and H_a represent the hardness values of the paracrystallites and amorphous regions respectively. From Fig. 6 it is clear that $H_c \gg H_a$. Hence

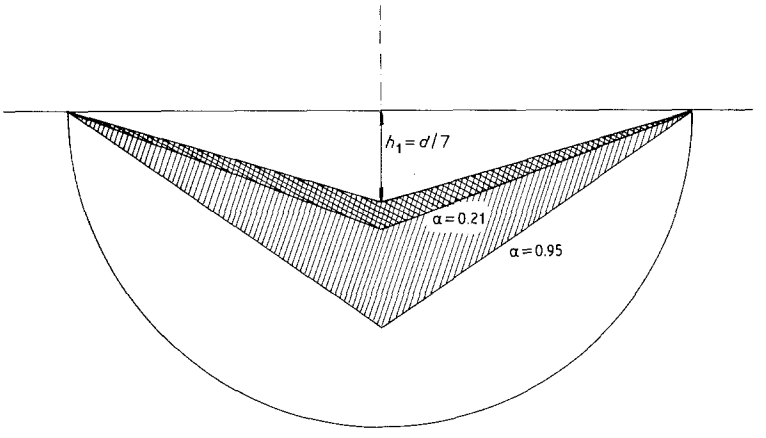

Figure 7 Strain boundaries for the lamellar destruction zone (assuming a pyramidal shape) round the Vickers indent for two PE samples with $\alpha = 0.95$ and $\alpha = 0.21$ respectively.

Equation 7 simplifies, to a first approximation to $MH = \alpha H_c$, thus, permitting a direct assessment of the microhardness of the crystals. One may inquire to what extent the crystal microhardness (stress needed to plastically deform the crystal) will be determined by the forces holding the chains together. Since we have shown that the inclusion of chain defects leads to a decrease of close chain packing within the lattice (Fig. 1) and to a concurrent increase of the lattice distortions it seems possible to expect, as a result, a decrease in the hardness of the crystals with increasing expansion of the lattice unit cell. Fig. 9 illustrates, indeed, the decreasing correlation between H_c and the cross-section $a \times b/2$. The extrapolation of the H_c data to 18.3 Å^2 (ideal lattice packing) offers a

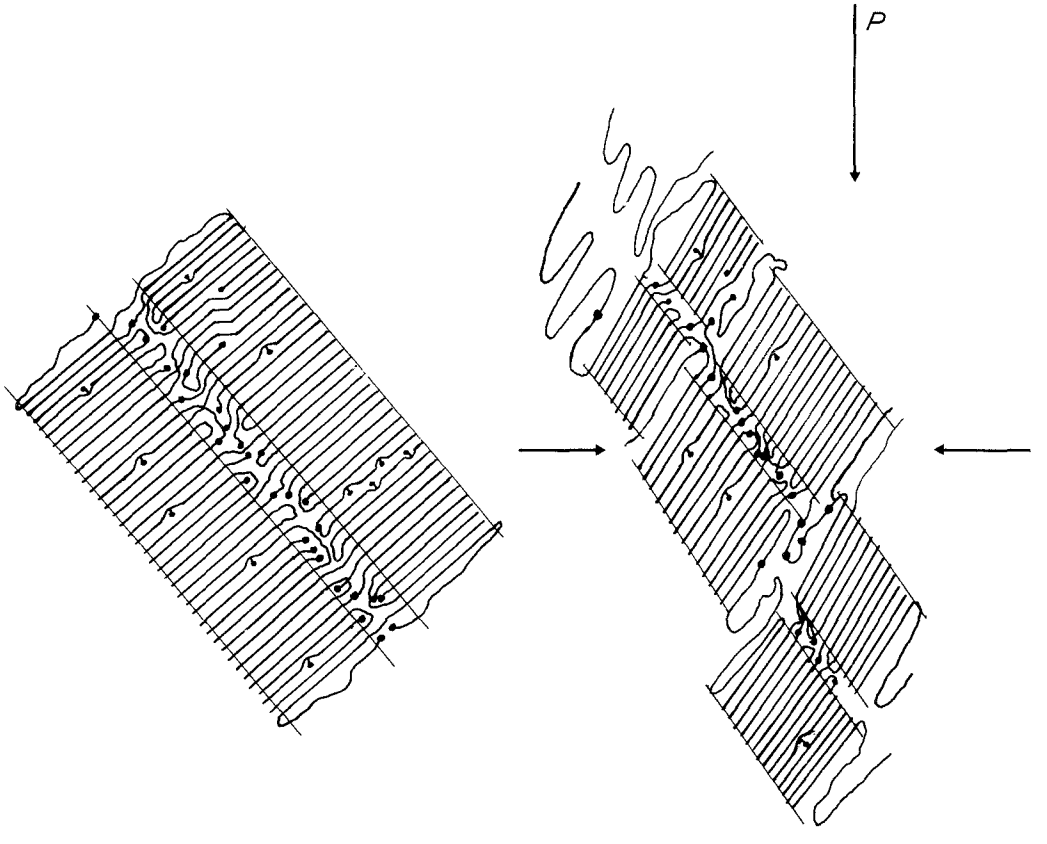

Figure 8 Suggested model for plastic deformation of the PE lamellar structure beneath the stress field of the indenter. The mosaic block structure of lamellae (left) introduces a weakness element allowing faster chain slip at block boundaries leading finally to a fracture (right).

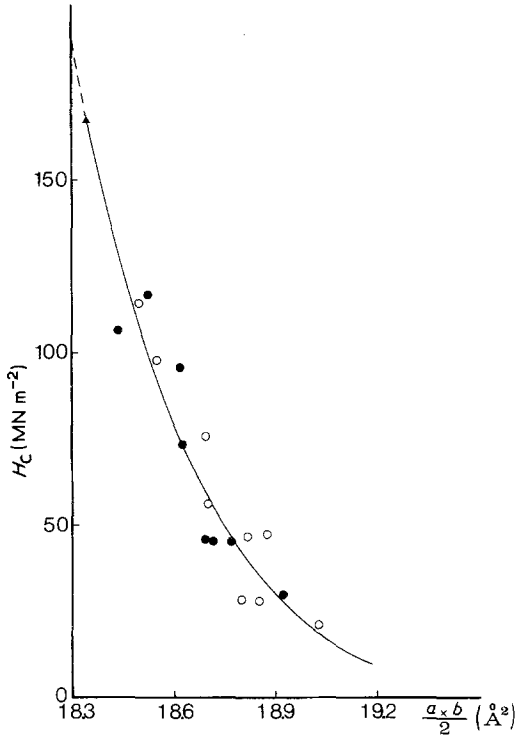

Figure 9 Microhardness of the "crystals" $H_c = MH/\alpha$, (for $t = 0.1$ min) against chain packing within the unit cell, • at $\Delta T \sim 10°$ C and ○ at $\Delta T \sim 68°$ C.

value of $-200\,MN\,m^{-2}$ which is in fair agreement with the value derived from the cohesive energy density based on van der Waals forces [12]. Thus, it may be concluded that the weak intermolecular forces are the ones that principally determine the micromechanical properties of the crystals. One should not forget, however, that the super-crystalline organization of the material i.e. stacks of lamellae in the microspherulitic structure with the amorphous component connecting the crystalline elements, confers an additional stability to the mechanical behaviour of the crystals [46]. Since the increase in molecular cross-section, $ab/2$, is linearly related to the reciprocal value of lamellae thickness [47, 48] the above data are consistent with the expected concurrent gradual increase of H_c with the crystal dimensions. We have shown in Figs 2, 3 and 5, that the preferential exclusion of defects from the crystal is, indeed, consistent with the clear simultaneous decrease of l and D with ϵ. The decrease in crystal hardness parallels, as a result, the decrease in the average volume of the mosaic blocks, V illustrated in Fig. 10. This is so because the thinner and the more imperfect the crystals, with a diminishing cohesion energy, the

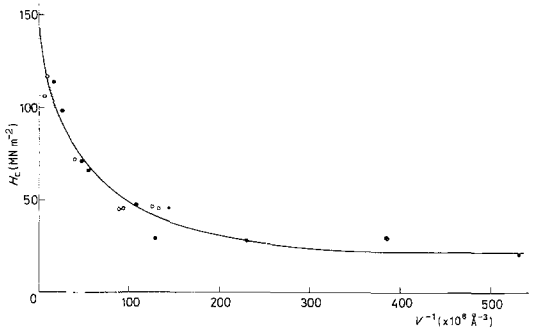

Figure 10 "Crystalline" microhardness (for $t = 0.1$ min) H_c against reciprocal value of the mosaic block volume $V = \pi xyl$, where x and y are the shape ellipsoid axes orthogonal to the $(h\,k\,0)$ planes [17].

lower is the resistance to plastic deformation. Fig. 10 additionally emphasizes the relevance of the physical dimensions of the mosaic blocks in determining the microhardness value of the lamellar structure.

In summarizing the data reported we can say that the increasing incorporation of defects within the lattice, causing an increase in the lattice distortions and inducing an enlargement of the value $a \times b/2$, impose a decrease of lateral size of the mosaic blocks according to Equation 6. The latter effect influences the size l of the crystals in the chain direction according to Wulf's relationship [48]. All these effects seem to be directly correlated to the overall decrease observed in the mechanical properties of the crystals.

4.2. Crystal destruction zone

For an ideal plastic material the mean pressure produced by a Vickers indenter is about 3 times the yield stress. As the yield stress of such a material is equal to its ultimate tensile strength we have a useful approximation between micro- and macroscopic mechanical properties. It is further known that macroscopic yielding of the polymer involves a local irreversible mechanism of fracture of the original paracrystalline blocks into smaller units [14]. Moreover, the heat generated during the destruction of lamellae gives so much chain mobilization in the blocks that they re-arrange to a new thickness determined by the temperature of deformation [45, 49, 50]. Since microindentation involves a similar yielding process it is conceivable to admit a certain destruction of lamellae localized at the material surface under the indenter eventually leading to a

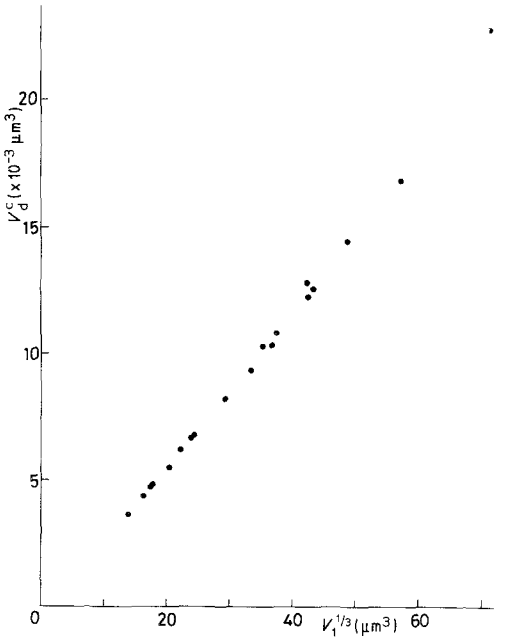

Figure 11 Volume of crystallites which are destroyed beneath the indenter, V_d^c as a function of the cubic root of the volume of the penetration within the sample calculated from Equation 10 for a load of 15 g at $t = 0.1$ min.

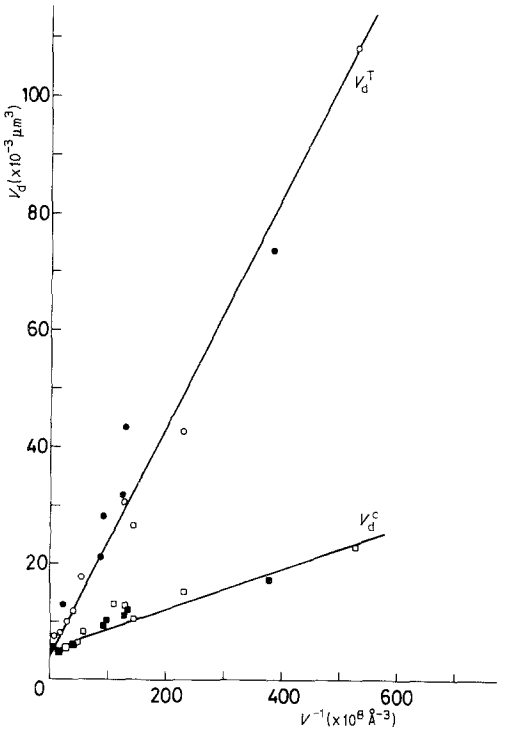

Figure 12 Total volume of material destroyed beneath the indenter V_d^T as compared with V_d^c against the reciprocal value of mosaic block volume, $P = 15$ g and $t = 0.1$ min.

"recrystallization" or rearrangement into a new crystalline structure even under deformation. This will be confirmed directly when experiments to observe lamellae changes after indentation are completed. It is, nevertheless, interesting to work out the volume of destroyed paracrystallites under the stress field of the indenter and evaluate the obtained data with regard to the geometry of the indenter and to the morphology of the system. By assuming that Wulf's rule, $D = \zeta l$, holds [16] the Gibbs free energy for the destruction, or "fusion", of a crystal with a thickness l can be written as [51]

$$\Delta\phi_c = -4l^2 \frac{\sigma^2}{\sigma_e} - 2l^2 \frac{\sigma^2}{\sigma_e} + \frac{3\sigma^2}{\sigma_e^2}(\Delta f) \quad (8)$$

where σ_e and σ are the fold and lateral surface free energies, respectively, and Δf is the bulk free energy of fusion. Assuming that $\sigma \simeq \sigma_e \sim 7.167\,10^{-7}$ cal cm^{-2} then the thermodyanical work per unit volume, $\Delta\phi$, to destroy a stacking of crystals with a given thickness l, turns out to be

$$\Delta\phi(\text{cal cm}^{-3}) = \frac{\Delta\phi_c}{l^2} \simeq -60l^{-1} + \Delta f. \quad (9)$$

This expression represents a hyperbolic decrease of $\Delta\phi$ with l. Hence, for a large crystal one obtains for the intercept $\Delta f \simeq 67$ cal cm^{-3}. Extrapolation of Equation 9 to $\Delta\phi = 0$ yields a crystallite thickness of 6.4 Å which agrees very well with the minimum number of methylene sequences in transconformation which would contribute to the absorption coefficient of the i.r. band at 720 cm^{-1} [52].

Furthermore, the mechanical work W performed under the indenter is equal to $W = ph$(cal); i.e. the load applied, p, times the penetration depth h. For the Vickers indenter $h = d/7$. Thus, $W = pd/7$(cal). To a first approximation we may assume that the work performed beneath the indenter is mainly consumed in crystal destruction. The much lower heat conductivity of the amorphous in contrast to the crystalline regions justifies this approximation [53]. Hence, the volume, V_d^c, of the crystallites which are destroyed under the indenter could be approximated to

$$V_d^c - \frac{W}{\Delta\phi} = \frac{pd}{7\Delta\phi}(\text{cm}^3). \quad (10)$$

On the other hand, since the volume, V_1, of material physically displaced under the Vickers pyramid, for a penetration depth h, is equal to

$$V_1 = K\frac{d^2h}{3} = K\frac{d^3}{21} \qquad (11)$$

then, one can anticipate that V_d^c will be proportional to $V_1^{1/3}$. The plot of Fig. 11 illustrates the nearly linear variation of the volume of destroyed crystallites V_d^c against the increasing cubic root of the volume V_1 of the indenter penetrating the sample. It is interesting to note that $V_d^c \ll V_1$. Furthermore, since the crystalline microhardness, H_c, is an increasing function of the average volume of the crystals (Fig. 10) and $MH \simeq f(1/h^2)$ it seems quite likely that V_d^c should be an inverse function of V. The nearly linear increase of V_d^c against the reciprocal crystal volume for the PE sample investigated is illustrated in Fig. 12. The total volume of destroyed material under the indenter including the non-crystalline regions $V_d^T = V_d^c\alpha^{-1}$ is also plotted here against V^{-1} for comparison. These results are consistent with the previous reciprocal relationship obtained between penetration depth of the indenter and crystal thickness [9].

In conclusion, for a constant applied load (in our case $P = 15$ g), the smaller are the PE paracrystallites and the larger becomes the volume displaced under the indenter V_1 and, as a result, the larger is the volume V_d^c of material destroyed. It is noteworthy, however, that for a given penetration depth the work W will be larger the harder the material (larger paracrystallites). V_d^T will be then, as a result, larger than for a softer material. Fig. 7 illustrates the boundaries of the volume zone of material destroyed round the Vickers indent (assumed to be pyramidal in shape) for h = constant, in the case of two samples with a crystallinity of $\alpha = 0.95$ (Rigidex chain extended crystals) ($l = 1650$ Å) and $\alpha = 0.21$ ($l = 36$ Å) respectively. It is clearly seen how the strain boundary of the zone of crystal destruction increases with both the crystal size and crystallinity of the material.

Acknowledgement

The "chain extended crystals" sample was kindly supplied by Dr D. C. Bassett, Reading.

References

1. D. TABOR, "The Hardness of Metals", Oxford, C. Press (1951).
2. H. O'NEILL, "Hardness Measurement of Metals and Alloys", (Chapman Hall, London, 1967).
3. B. MAXWELL, *Mod. Plast.* **32** (1955) 125.
4. E. BAER, R. E. MAIER and R. N. PETERSON, *SPE J.* **17** (1961) 1203.
5. K. MÜLLER, *Kuntstoffe* **60** (1970) 265.
6. H. H. RACKÉ and T. FETT, *Materialprüfung* **13** (1971) 37.
7. P. EYERER and G. LANG, *Kuntstoffe* **62** (1972) 322.
8. J. BOWMAN, N. HARRIS and M. BEVIS, *J. Mater. Sci.* **10** (1975) 63.
9. F. J. BALTÁ CALLEJA, *Colloid Polymer Sci.* **254** (1976) 258.
10. F. J. BALTÁ CALLEJA and D. C. BASSETT, *J. Polymer Sci. Polymer Sym.* **58** (1977) 157.
11. J. BOWMAN and M. BEVIS, *Colloid Polymer Sci.* **256** (1977) 954.
12. F. J. BALTÁ CALLEJA, D. R. RUEDA, R. S. PORTER and W. T. MEAD, *J. Mater. Sci.* **15** (1980) 765.
13. F. J. BALTÁ CALLEJA, W. T. MEAD and R. S. PORTER, *Polymer Eng. Sci.* **20** (1980) 393.
14. A. PETERLIN, *J. Mater. Sci.* **6** (1971) 490.
15. D. T. GRUBB and A. KELLER, *J. Polymer Sci. Polymer Phys. Ed.* **18** (1980) 207.
16. H. ČAČKOVIĆ, R. HOSEMANN and W. WILKE, *Kolloid Z. Z. Polym.* **234** (1969) 1000.
17. J. MARTINEZ SALAZAR and F. J. BALTÁ CALLEJA, *J. Cryst. Growth* **48** (1980) 283.
18. I. R. HARRISON, A. KELLER, D. M. SADLER and E. L. THOMAS, *Polymer* **17** (1976) 736.
19. J. HAASE, R. HOSEMANN and H. ČAČKOVIĆ, *ibid.* **18** (1977) 734.
20. W. PECHHOLD and S. BLASENBREY, *Kolloid Z. Z. Polym.* **235** (1967) 216.
21. F. J. BALTÁ CALLEJA, J. C. GONZALEZ ORTEGA and J. MARTINEZ SALAZAR, *Polymer* **19** (1978) 1094.
22. F. J. BALTÁ CALLEJA and R. HOSEMANN, *J. Polymer Sci. Polymer Phys. Ed.* **18** (1980) 1159.
23. H. ČAČKOVIĆ, J. LOBODA-ČAČKOVIĆ, R. HOSEMANN and D. WEICK, *Colloid Polymer Sci.* **252** (1974) 812.
24. D. R. RUEDA, F. J. BALTÁ CALLEJA and A. HIDALGO, *Spectrochim. Acta* **30A** (1974) 1545.
25. *Idem, ibid.* **35A** (1979) 847.
26. J. C. GONZALEZ ORTEGA and F. J. BALTÁ CALLEJA, *An. Fiz.* **70** (1974) 92.
27. C. G. VONK, *J. Appl. Cryst.* **6** (1973) 148.
28. R. HOSEMANN and S. N. BAGCHI, "Direct Analysis of Diffraction by Matter" (North Holland, Amsterdam, 1962) pp. 239–46.
29. J. MARTINEZ SALAZAR and F. J. BALTÁ CALLEJA, *Polymer Bull.* **2** (1980) 163.
30. W. GLENZ, N. MOROSOFF and A. PETERLIN, *Polymer Lett.* **9** (1971) 211.
31. P. R. SWAN, *J. Polymer Sci.* **56** (1962) 409.
32. P. J. HOLDSWORTH and A. KELLER, *Polymer Lett.* **5** (1967) 605.
33. G. T. DAVIS, R. K. EBY and G. M. MARTIN, *J. Appl. Phys.* **39** (1968) 4973.
34. R. HOSEMANN and F. J. BALTÁ CALLEJA, *Ber. Bunsenges. Phys. Chem.* **84** (1980) 91.
35. R. HOSEMANN, CRC Critical Rev. Macromol. Sci. October (1972) 351.

36. G. W. EHRENSTEIN, *Kunststoffe* **66** (1975) 289.
37. E. H. ANDREWS, *Pure Appl. Chem.* **39** (1974) 179.
38. L. E. NIELSEN, *J. Appl. Phys.* **25** (1954) 1209.
39. F. P. REDING, *J. Polymer Sci.* **32** (1958) 487.
40. G. R. WILLIAMSON, B. WRIGHT and R. N. HOWARD, *J. Appl. Chem.* **14** (1964) 131.
41. P. B. BOWDEN, *Polymer* **9** (1968) 449.
42. R. HOSEMANN, J. LOBODA-ČAČKOVIĆ and H. ČAČKOVIĆ, *Colloid Polymer Sci.* **254** (1976) 782.
43. H. KIHO, A PETERLIN and P. H. GEIL, *J. Appl. Phys.* **35** (1964) 1599.
44. J. R. WHITE, *J. Polymer Sci. Polymer Phys.* **16** (1978) 387.
45. A. PETERLIN and F. J. BALTÁ CALLEJA, *Kolloid Z. Z. Polym.* **242** (1970) 1093.
46. A. PETERLIN, *Macromol. Chem.* 8 (1973) 277.
47. G. T. DAVIS, J. J. WEEKS, G. M. MARTIN and R. K. EBY, *J. Appl. Phys.* **45** (1974) 4175.
48. R. HOSEMANN and F. J. BALTÁ CALLEJA, *Polymer* **20** (1979) 1091.
49. F. J. BALTÁ CALLEJA, A. PETERLIN and B. CRIST, *J. Polymer Sci. A2* **10** (1972) 1749.
50. J. LOBODA-ČAČKOVIĆ, H. ČAČKOVIĆ and R. HOSEMANN, *J. Macromol. Sci. Phys.* **B16(1)** (1979) 127.
51. J. D. HOFFMANN, G. T. DAVIS and J. I. LAURITZEN Jr, in "Treatise on Solid State Chemistry", Vol. 3, edited by N. B. Hannay (Plenum Press, New York, 1976) p. 528.
52. D. R. RUEDA, F. J. BALTÁ CALLEJA and A. HIDALGO, *J. Polymer Sci. Polymer Phys. Ed.* **15** (1977) 2027.
53. A. GALESKI, P. MILCZAREK and M. KRYSZEWSKI, *ibid.* **15** (1977) 1267.

Received 26 June and accepted 7 August 1980.